Estuaries and Coasts (2020) 43:722–738
https://doi.org/10.1007/s12237-020-00697-1

Frontogenesis at Estuarine Junctions

W. Bryce Corlett [1,2,3] · W. Rockwell Geyer [1]

Received: 6 November 2018 / Revised: 25 October 2019 / Accepted: 3 January 2020 / Published online: 30 January 2020

Abstract
Observations of Newark Bay, a sub-estuary network characterized by multiple junctions, reveal that fronts are generated by tidal flow through transitions in channel geometry. All fronts substantially contribute to along-channel estuarine heterogeneity, and most are associated with both changes in channel geometry and tidal velocity phase-shifts. A lift-off front forms at the mouth of the sub-estuary during ebb tide in response to the abrupt seaward channel expansion. While forming, the front is enhanced by a tidal velocity phase-shift; flood tide persists in the main estuary until 90 min after the start of ebb tide in the sub-estuary. A second lift-off front forms during ebb tide at a channel–side-channel junction and is enhanced by a lateral baroclinic circulation induced by baroclinic and barotropic tidal velocity phase-shifts between the main channel and side channel. The lateral circulation also bifurcates the along-channel ebb flow at the surface, generating a surface front above the lift-off front. At the head of Newark Bay, a second surface front forms during ebb tide at the confluence of two tributary estuaries. This confluence front is rotated across the mouth of the primary fresh water source by high velocities from the adjacent tributary estuary and is maintained through much of ebb tide by lateral straining and mixing. Although the overall stratification of Newark Bay would categorize it as a partially mixed estuary, the fronts divide the density structure of the sub-estuary into a series of nearly homogeneous segments—a characteristic that is more often associated with fjords.

Keywords Salinity front · Frontogenesis · Sub-estuary · Junction · Confluence

Introduction

Partially mixed estuaries are often portrayed as having near-uniform along-channel salinity and stratification gradients (Hansen and Rattray Jr. 1965; MacCready and Geyer 2010). However, observations frequently reveal significant variability in the strength of these gradients, especially in fjords. In Puget Sound, for example, horizontal gradients in salinity and stratification are larger over shallow sills than along deep basins (Ebbesmeyer and Barnes 1980). At bathymetric transitions, horizontal salinity gradients are concentrated in fronts on tidal timescales (Lavelle et al. 1991). These recurring salinity fronts divide the fjord into a series of distinct tidal-residual segments (Cokelet and Stewart 1985). The characteristics of fjords that are associated with fronts, such as along-channel heterogeneity, may also be relevant to partially mixed and well-mixed estuarine regimes, as fronts form in all types of estuaries (Largier 1993; Geyer and Ralston 2015).

Along-channel estuarine fronts are generated by a variety of mechanisms, which are manifest in the tendency equation of the along-channel salinity gradient, derived from the along-estuary derivative of the salt conservation equation:

$$\underbrace{\frac{\partial}{\partial t}\frac{\partial s}{\partial x}}_{1}+\underbrace{\vec{u}\cdot\nabla\frac{\partial s}{\partial x}}_{2}=-\underbrace{\frac{\partial u}{\partial x}\frac{\partial s}{\partial x}}_{3}-\underbrace{\frac{\partial v}{\partial x}\frac{\partial s}{\partial y}}_{4}-\underbrace{\frac{\partial w}{\partial x}\frac{\partial s}{\partial z}}_{5}-\underbrace{\frac{\partial}{\partial x}\frac{\partial\overline{(s'w')}}{\partial z}}_{6} \quad (1)$$

This equation describes the tendency (term 1) and advection (term 2) of the local salinity gradient, as well as the generation of along-channel fronts through the convergence of the along-channel salinity gradient (term 3), the twisting of a cross-channel gradient (term 4), the shearing of stratification (term 5), and the sharpening of the along-channel salinity gradient by a mixing gradient (term 6). This equation can also describe the destruction of an along-channel front through the

Communicated by William Boicourt

✉ W. Bryce Corlett
bcorlett@moffattnichol.com

[1] Woods Hole Oceanographic Institution, Woods Hole, MA, USA

[2] MIT-WHOI Joint Program in Oceanography/Applied Ocean Science and Engineering, Cambridge, MA, USA

[3] Moffatt & Nichol, Costa Mesa, CA, USA

reversal of processes described above. For example, term 3 can describe either front generation by an along-channel convergence or front destruction by an along-channel divergence, depending on the directions of the salinity and horizontal velocity gradients. Although all of these mechanisms may generate fronts, frontogenesis by along-channel convergence is most commonly discussed (Simpson and Nunes 1981; Largier 1992; MacDonald and Geyer 2005; Ralston et al. 2010).

The formation of along-channel convergence fronts was first investigated by Simpson and Linden (1989). Through a series of lock exchange experiments, they determined that convergences may be generated by locally intensified horizontal salinity gradients. The locally intensified horizontal pressure gradient, in turn, produces an along-channel convergence. In a modeling study of the Hudson estuary, Geyer and Ralston (2015) demonstrated that frontogenesis may also occur at channel expansions, where velocity convergences are produced by the hydraulic response of stratified flow to the change in width or depth. During ebb tide, stratified flow lifts off from the bed at seaward channel expansions, generating along-channel convergences between rapid ebb flow on the landward side of the lift-off zone and stagnant or weakly ebbing flow on the seaward side (Horner-Devine et al. 2015). This convergence concentrates the along-channel salinity gradient at the bed in a lift-off front (Geyer and Ralston 2015).

During flood tide, on the other hand, the buoyant surface layer is often arrested by saline inflow at landward channel expansions (Simpson and Nunes 1981; Huzzey 1982). The inflow subducts beneath the surface layer, generating a velocity convergence between inflow on the seaward side of the plunge line and nearly stagnant flow on the landward side (Largier 1992; Marmorino and Trump 1996). This convergence concentrates the surface salinity gradient in a tidal intrusion front. During formation, both lift-off fronts and tidal intrusion fronts are essentially arrested gravity currents (Benjamin 1968; Pelegri 1988), in which the baroclinic propagation speed of the front matches the speed of the oncoming flow. Consequently, the internal hydraulic state of the flow is often critical at locations of frontogenesis (Armi and Farmer 1986).

Lift-off fronts and tidal intrusion fronts also share similar propagation characteristics. Lift-off fronts tend to propagate landward as gravity currents after the change of tide; Geyer and Farmer (1989), for example, described the landward propagation of a lift-off front as a salt wedge during flood tide at the mouth of the Fraser River. In some cases, these propagating fronts induce the formation of new bottom fronts during the following ebb tide by initiating along-channel convergences at more landward locations (Simpson and Linden 1989). Tidal intrusion fronts may propagate after the change of tide as well; these fronts propagate seaward during ebb tide, and in some cases leave estuaries as plume fronts (Nunes 1982). However, tidal intrusion fronts may also propagate after initially forming during flood tide. For instance, Brubaker and Simpson (1999) observed that these fronts may be advected landward from bathymetric transitions and dissipate as flood tide intensifies.

Fronts also form at bathymetric transitions through non-buoyant processes. At channel confluences, for example, laterally convergent streams produce fronts (Best 1987; Rhoads and Sukhodolov 2001). When the confluence is asymmetric, i.e., one of the flows is stronger than the other, the resulting lateral shear may rotate the front into the along-channel direction (De Serres et al. 1999; Riley et al. 2014). These fronts may also exhibit cross-front buoyancy gradients, which are produced by either contrasting water properties (Farmer et al. 1995) or tidal phase-shifts between channels (Warner et al. 2002; Giddings et al. 2012).

Confluence fronts, lift-off fronts, and tidal intrusion fronts each form at channel junctions, located either within an estuary or between an estuary and the receiving waters (e.g., lift-off fronts). These junctions provide either the geometry or spatial shifts in tidal current phase (the relationship between tidal height and velocity) that are conducive to frontogenesis. Spatial shifts in tidal current phase at junctions may also modify the process of frontogenesis by altering the horizontal salinity gradient (Pritchard and Bunce 1959; Alebregtse et al. 2013) and the along-channel velocity gradient (Warner et al. 2003). Warner et al. (2002), for example, observed that the phasing of tidal currents between channels can generate either convergent or divergent along-channel salinity gradients at a junction depending on the phase of the tide. A similar phase-shift at a junction between a channel and side channel may enhance the lateral salinity gradient, generating a lateral bottom front (van Maren et al. 2009). These bottom fronts propagate into side channels as part of a tidal lock exchange process produced by the channel—side channel phase-shift (Allen and Price 1959; Hayward et al. 1982). The lock exchange may also influence the along-channel salinity gradient by alternately exporting freshwater into the main channel at the surface and saline water into the channel at the bed.

In this observational study, we examine how junctions affect the formation of salinity fronts in the Newark Bay subestuary, and how these fronts contribute to a heterogeneous estuarine structure. The structure of the paper is as follows: the second section describes the site; the third section reports our observation methods; the fourth section analyzes the influence of junctions on the formation of salinity fronts; and the fifth section discusses the effects of fronts on the heterogeneity of the Newark Bay sub-estuary.

Methods

Site

Newark Bay, New Jersey, is a sub-estuary of the Hudson River—New York Harbor estuary (Fig. 1). The sub-estuary is connected to the Harbor through Kill van Kull and to Raritan Bay (another sub-estuary of the estuarine network) through a narrow tidal strait called Arthur Kill. New York Harbor and each of the connecting straits are roughly 20 m deep. At the junction between the Harbor and Kill van Kull, the width of the channel abruptly decreases by one third. The channel is further punctuated by a series of abrupt bathymetric transitions within the sub-estuary, which are due to the natural geometry of the system as well as human-induced channel modifications. These modifications include two side channels associated with Port Newark and Port Elizabeth and an abrupt shoaling of the channel from 17 to 13 m in the middle of Newark Bay. At the northern end of Newark Bay, the channel splits into the Passaic and Hackensack rivers; the channel shoals from 13 to 6 m at the mouth of the Passaic.

Tides within the sub-estuary are largely semidiurnal, with a mean range of 1.5 m (Mathew and Winterwerp 2017). Tidal velocity and water level are 90° out of phase throughout the sub-estuary (Chant et al. 2011). Tidal velocity and water level are 45° out of phase in the adjacent Hudson River (Nepf and Geyer 1996); consequently, tidal velocities within the Harbor lag velocities within the sub-estuary by 45°, or roughly 90 min. Newark Bay is a partially mixed estuary, with modest to moderate stratification and a robust two-layer estuarine exchange flow (Suszkowski 1978; Chant et al. 2018). Most freshwater (85%) enters the sub-estuary from the Passaic River; however, the Passaic River tidal prism is roughly one quarter of the size of the Hackensack River tidal prism (Shrestha et al. 2014). Most seawater enters the sub-estuary through Kill van Kull, in response to a net clockwise circulation around Staten Island (Suszkowski 1978; Blumberg et al. 1999). This circulation pattern is produced by a mean sea level gradient between the mouth of Kill van Kull in New York Harbor and the mouth of Arthur Kill in Raritan Bay (Kaluarachchi et al. 2003).

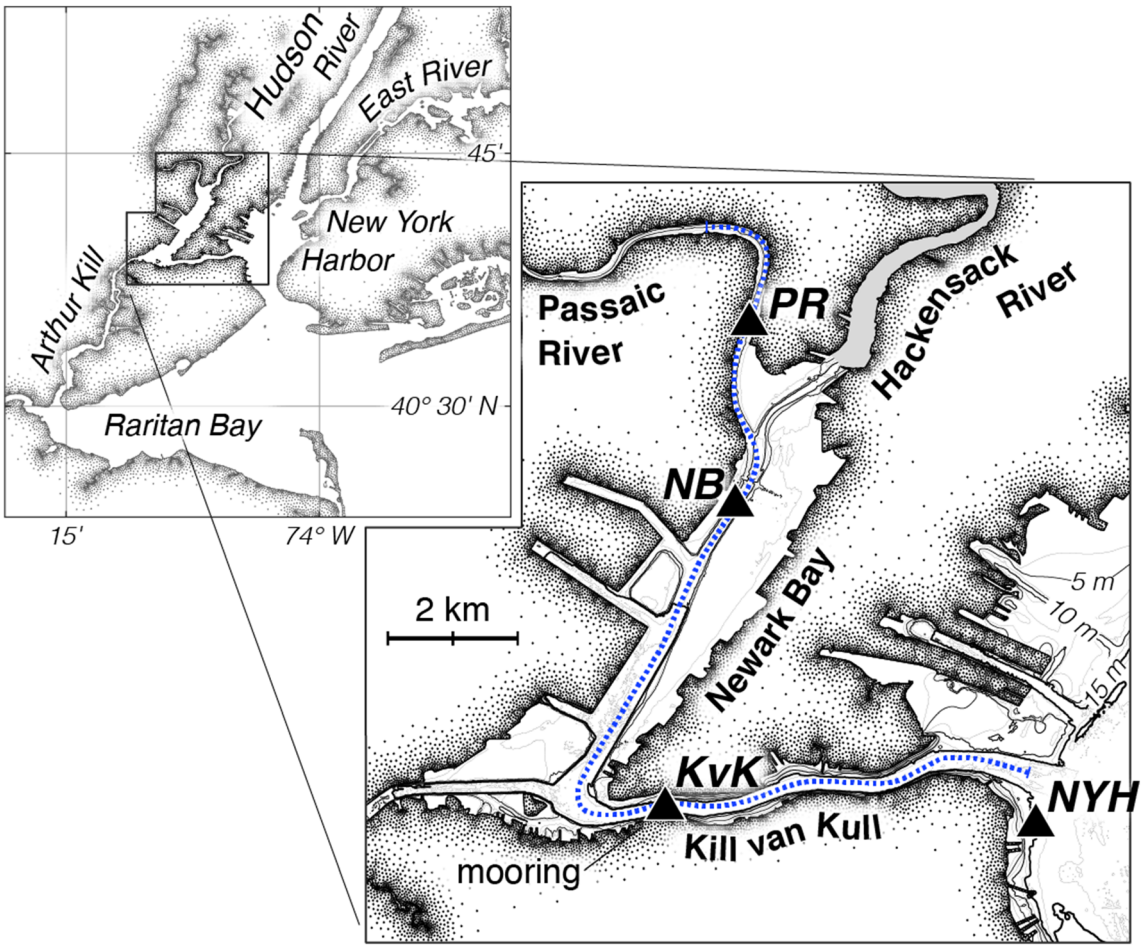

Fig. 1 The Newark Bay sub-estuary, showing locations of moorings and the along-channel hydrographic sections. The inset depicts the surrounding waterways

Observations

Shipboard and moored observations of the Newark Bay sub-estuary and New York Harbor were conducted in the spring and early summer of 2016. From March 17 through July 5, four moorings were deployed along the axis of the sub-estuary, each within a region of distinctly different channel geometry (Fig. 1). From south to north, these moorings are labeled New York Harbor (*NYH*), Kill van Kull (*KvK*), Newark Bay (*NB*), and Passaic River (*PR*). All moorings were equipped with near-bed and near-surface RBR conductivity-temperature-depth (CTD) sensors; near-bed CTD sensors were mounted 0.5 m above the bed and near-surface sensors were mounted 1 m below the water surface. All CTD sensors sampled water properties once per minute. Moorings *NYH* and *NB* were also equipped with bottom-mounted 1 MHz Nortek AWAC acoustic Doppler current profilers (ADCPs), which measured velocities in 0.5 m depth bins throughout the water column every 10 min; the center of the bottom depth bin was located roughly 1.75 m above the bed. Mooring *KvK* was equipped with a bottom-mounted 600 kHz RDI ADCP, which measured velocities in 0.5 m depth bins throughout the water column every 15 min; the center of the bottom depth bin of the ADCP was located 1.6 m above the bed. Mooring *PR* was equipped with a 2-MHz Nortek Aquadopp ADCP, though data from this ADCP was not recovered due to corrosion by sea water; while deployed, the housing was breached by a propeller. Some loss of CTD data occurred at all moorings due to biofouling. Consequently, comprehensive data coverage of the sub-estuary with moored instruments ceased on May 30. All mooring-based data were interpolated onto a 10-min sampling interval for processing and analyses.

To capture the along-channel variability of estuarine characteristics, shipboard measurements of velocity and salinity were made over semidiurnal tidal periods using a downward-facing 1200 kHz RDI ADCP and continuously profiling RBR CTDs while traversing transects at roughly 3 m/s. The ADCP measured velocities throughout the water column in 0.25 m depth bins once per second; the average horizontal resolution is equivalent to one profile every 2.5 m. The CTDs measured water properties at a rate of 12 Hz, producing salinity profiles with a vertical resolution of 0.1 m roughly every 70 m along the channel. For analyses of shipboard measurements, data were subsampled onto the vertical resolution of ADCP measurements and the horizontal resolution of CTD measurements. Shipboard surveys took place during two periods of the mooring deployment. The first period (May 11–14) coincided with larger-than-average (perigean) spring tides and relatively high discharge conditions (Fig. 2, top panel), and the second (June 30—July 1) occurred during smaller (apogean) spring tides and low discharge conditions. All sections fall along the transect shown in Fig. 1, which follows the primary axis of the sub-estuary from *NYH* to *PR*.

Results

Overall Structure and Variability

During the observation period, mean discharge from the Passaic and Hackensack rivers was 15 m^3/s (Fig. 2, top panel)—the 42nd percentile of the overall historical record and the 6th percentile of the seasonal climatology (USGS gages 01389500 and 01378500, 1920–2015). Freshwater discharge in the adjacent Hudson River estuary was above average relative to overall historical conditions, but below average relative to the seasonal climatology (at the 66th and 9th percentiles, respectively; USGS gage 01358000, 1946–2015). The tidal range within the sub-estuary was larger than average during the observation period; the alignment of lunar perigee with spring tides produced two perigean springs and three apogean springs (Fig. 2, bottom panel). Tidal water level amplitudes ranged from roughly 0.5 m during neap tides to 1.0 m during perigean spring tides. Mean tidal velocities within the sub-estuary ranged from 0.5 to 0.9 m/s over the same period.

The salinity time series at the moorings exhibit variations due to the tides, spring/neap modulations, and fluctuations in river flow (Fig. 2). In New York Harbor, the spring/neap cycle significantly influences subtidal surface salinity variability; the surface of the Harbor is up to 10 psu fresher during neap tides than during perigean spring tides. Within the sub-estuary, the influence of the spring/neap cycle is more evident in near-bed salinity variability, although the response rapidly weakens toward the head of the sub-estuary. In the Passaic River, subtidal salinity variability is strongly influenced by fluctuations in river flow. Tidal salinity variability is most notable at moorings *PR* and *NYH*; however, all moorings exhibit rapid tidal salinity fluctuations. The varying tidal signal between moorings indicates that the strength of the horizontal salinity gradient changes over scales less than the tidal excursion.

Spatial Structure

The spatial heterogeneity of salinity and stratification is confirmed by an along-channel salinity section obtained at the end of ebb tide (Fig. 3). Although the section presents a snapshot of tidal conditions, its depiction of the sub-estuary is consistent with the mean characteristics of the moored time series. Stratification is largest at the landward and seaward boundaries of the sub-estuary. Conditions within Newark Bay are partially mixed, and Kill van Kull is largely well-mixed. Between regions of different stratification, the along-channel

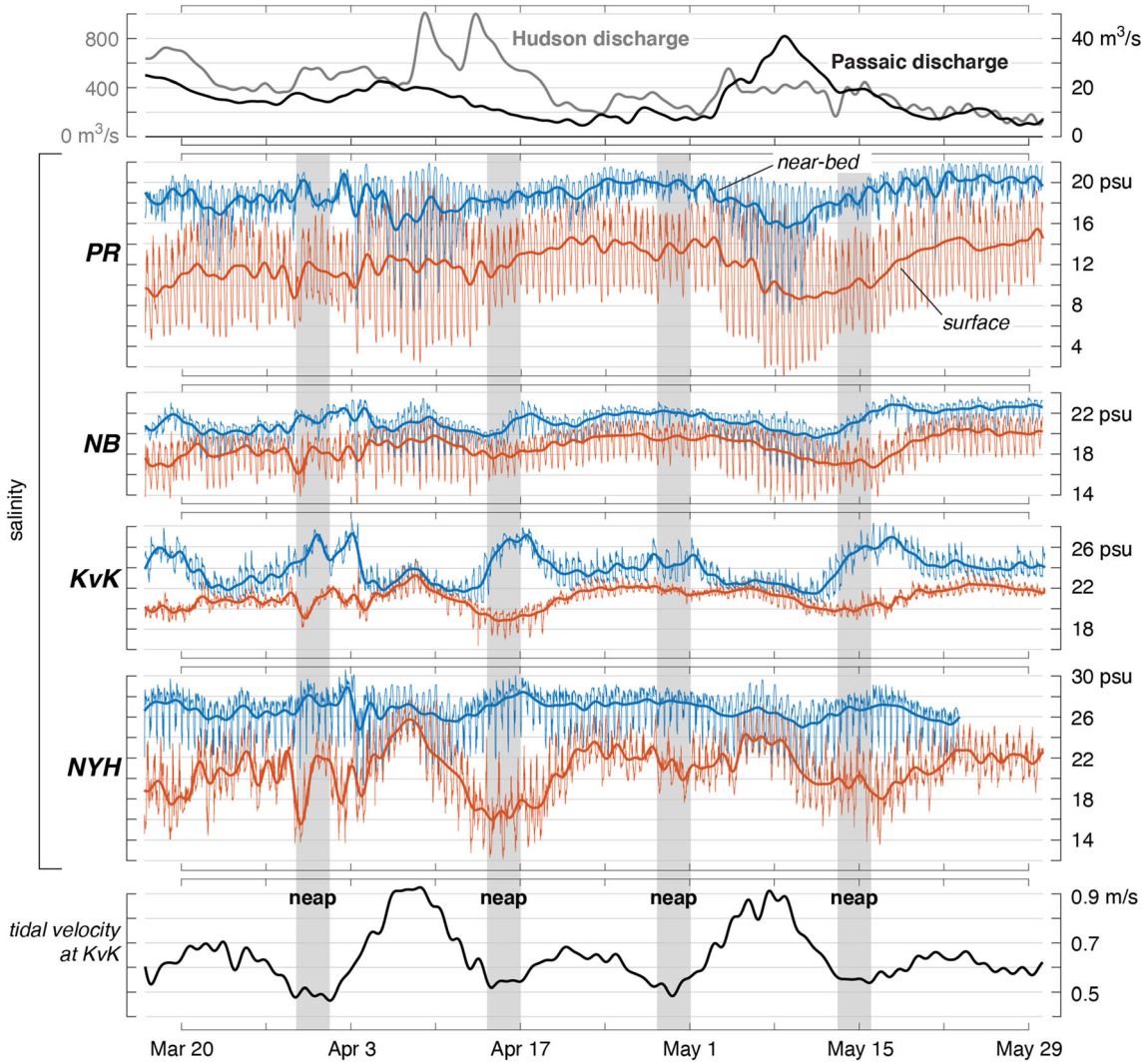

Fig. 2 Time series of environmental conditions and salinity over the period of full moored data coverage. Tidal velocity refers to the average magnitude of the maximum depth-averaged flood and ebb velocities over a tidal cycle. 33-h filtered salinity measurements are superimposed over 10-min data to show subtidal variability

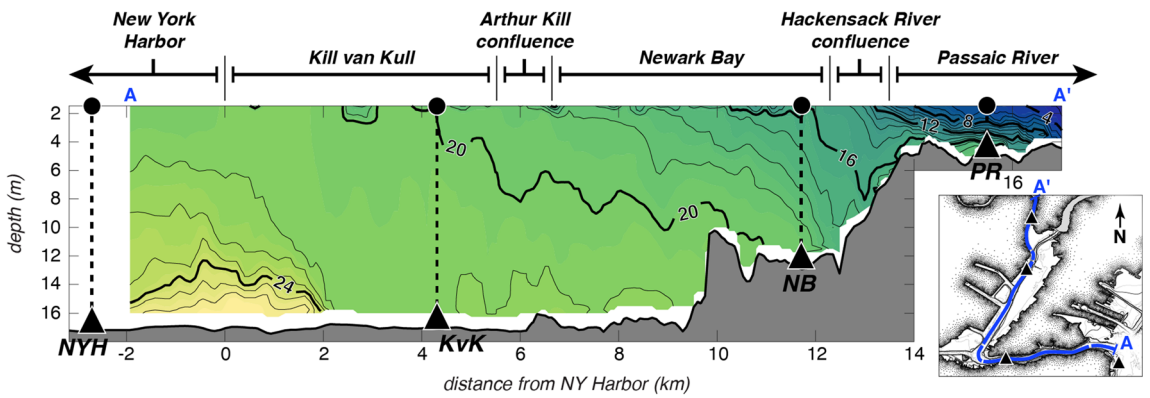

Fig. 3 Mooring locations relative to the end-of-ebb along-channel salinity structure of the sub-estuary during spring tides and high discharge. Isohalines are indicated with both black contour lines and color shading

salinity gradient is concentrated in fronts. A bottom front at the mouth of the sub-estuary separates the Harbor from Kill van Kull, and a surface front separates the Passaic River from the Hackensack River confluence. Salinity and stratification gradients are more gradual between Kill van Kull and Newark Bay; however, a weak bottom front is observed near 12 km, and a weak surface front is observed near 10 km.

Temporal Evidence of Fronts

The salinity measured at each mooring rapidly increases during flood tide, consistent with the passage of fronts (Fig. 4). Both surface and bottom fronts that are advected landward during flood tide produce rapid increases in salinity at a stationary mooring, as the sharp horizontal salinity gradients are translated into rapid temporal changes in salinity. The rapid increases in salinity in the moored observation records that are associated with the passage of fronts are at least two standard deviations larger than the mean temporal salinity gradient. The tidal cycles at each mooring that contain these rapid changes in salinity are shown in gray in Fig. 4; repeated hydrographic sections (discussed in the "Formation and Evolution of Fronts" section) confirm that these tidal fluctuations are indeed generated by advected bottom and surface salinity fronts. To emphasize the characteristics of the fronts, the tidal salinity time series shown in Fig. 4 are aligned such that all rapid increases in salinity occur at the mean tidal hour of frontal advection at each mooring. The average tidal salinity variability at each mooring after co-locating frontal measurements is shown in black. This process of identifying advected fronts within the moored salinity records reveals that bottom fronts pass moorings *KvK* and *NB* in over 70% of tidal cycles, and surface fronts pass moorings *PR* and *NB* in over 90% of tidal cycles.

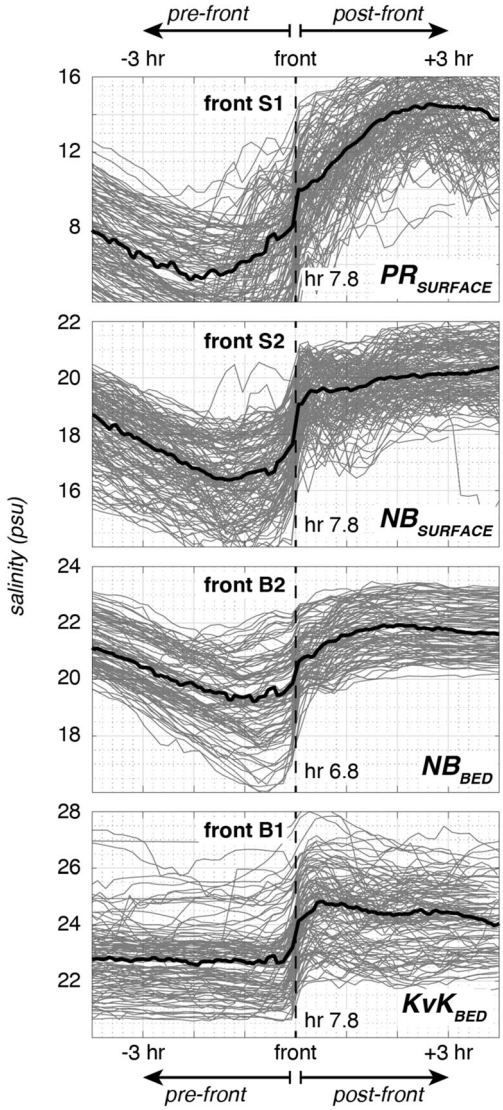

Fig. 4 Temporal increases in salinity attributed to the landward advection of fronts at each mooring. Time series are aligned such that all fronts occur at the mean tidal hour of frontal advection. Tidal hours are given in reference to the depth-averaged velocity at each mooring; hour 0 occurs at the start of ebb tide, and hour 6 occurs at the start of flood tide. Note that the salinity scale at mooring *PR* is twice as large as the scales at moorings *NB* and *KvK*

The consistent observations of frontal advection throughout the three-month record permit the characterization of the fronts at each mooring. At mooring *KvK*, the recurrent bottom front (labeled B1) increases near-bed salinity by an average of 2 psu in early flood tide. The salinity difference across the front fluctuates over the observation record by less than 1 psu. The large subtidal salinity fluctuations evident in Fig. 4 are instead produced by the effects of the spring/neap cycle on the mean tidal salinity at the mooring; the mean flood tide salinity at mooring *KvK* decreases by roughly 3 psu from neap tides to perigean spring tides. Front B1 passes the mooring by 2 h into flood tide on average, which suggests that the front originates roughly 2.5 km seaward of the mooring, assuming that the front is primarily advected by depth-averaged tidal velocities. This location is consistent with the observed location of the bottom front in Kill van Kull in Fig. 3. However, the salinity gradient across the front in the mooring observations is much weaker than the salinity gradient across the front in the hydrography. This suggests that the front is significantly modified by tidal processes before passing mooring *KvK*.

The recurring bottom front in Newark Bay (labeled B2) increases the near-bed salinity at mooring *NB* by an average of 2 psu roughly 30 min after the start of flood tide. The salinity difference across the front is significantly influenced by spring/neap variability; the difference in salinity across front B2 increases by an average of 1.7 psu from neap tides to perigean spring tides. The relationship between the strength of the front and the spring/neap cycle suggests that the process of frontogenesis for front B2 is influenced by the tidal salinity range. The time at which the bottom front (B2) passes the mooring, conversely, fluctuates nearly independently of spring/neap and discharge variability; most measurements of

the front occur 20–70 min after the start of flood. This range suggests that the front forms roughly 0.5 km downstream of the mooring, assuming that the front is advected landward by near-bed velocities similar to those observed at the mooring.

The recurring surface front at mooring *NB* (labeled front S1) increases the surface salinity by an average of 3 psu in early flood tide. The salinity difference across this front is similarly influenced by the spring/neap cycle, increasing by an average of 1.7 psu from neap tides to perigean spring tides. This suggests that the process of formation for this front is influenced by the tidal salinity range. The time at which the front passes the mooring also fluctuates over the spring/neap cycle, decreasing from 2.2 to 1.4 h into flood from neap tides to perigean spring tides. This suggests that the front consistently forms in the same location, at most 2.5 km seaward of the mooring, assuming that the front forms at the start of flood tide and is advected landward by tidal velocities.

The surface front at mooring *PR* increases the near-surface salinity by an average of 7 psu in early flood tide, which is consistent with the salinity difference across the front observed at the mouth of the Passaic River in Fig. 3. At the mooring, the salinity difference across the front ranges from 2 to 14 psu over the observation record, producing the vertical spread of salinity measurements shown in Fig. 4. Most of this variability is due to fluctuations in river flow; the salinity difference increases from an average of 4 psu during low discharge to 8 psu during peak discharge. The front is typically observed 2 h after the start of flood tide, although the time of observation does fluctuate from tide to tide; most observations of front S2 occur between 1.3 and 2.4 h into flood tide.

Formation and Evolution of Fronts

Repeated hydrographic surveys in each region of the sub-estuary provide insight into the formation and evolution of these fronts. All fronts observed at the moorings form at junctions during ebb tide. The fronts are generated by flow through the junctions, and most are modified by tidal phase-shifts. While there are similarities among the frontal locations, each front demonstrates a different mechanism through which junctions influence frontogenesis and frontal evolution.

Front B1

The formation and evolution of bottom front B1 is shown in 2-h intervals in Fig. 5. At the start of ebb tide (hour 0.7), the near-bed salinity gradient within Kill van Kull is nearly uniform. Ebb flow accelerates seaward at the 500-m channel expansion at the mouth of the sub-estuary (0 km). Although the sub-estuary is beginning to ebb at hour 0.7, the Harbor continues to flood; this phase-shift is evident in the landward near-bed flow observed 2 km seaward of the mouth of Kill van Kull, which opposes the strengthening ebb in the sub-estuary.

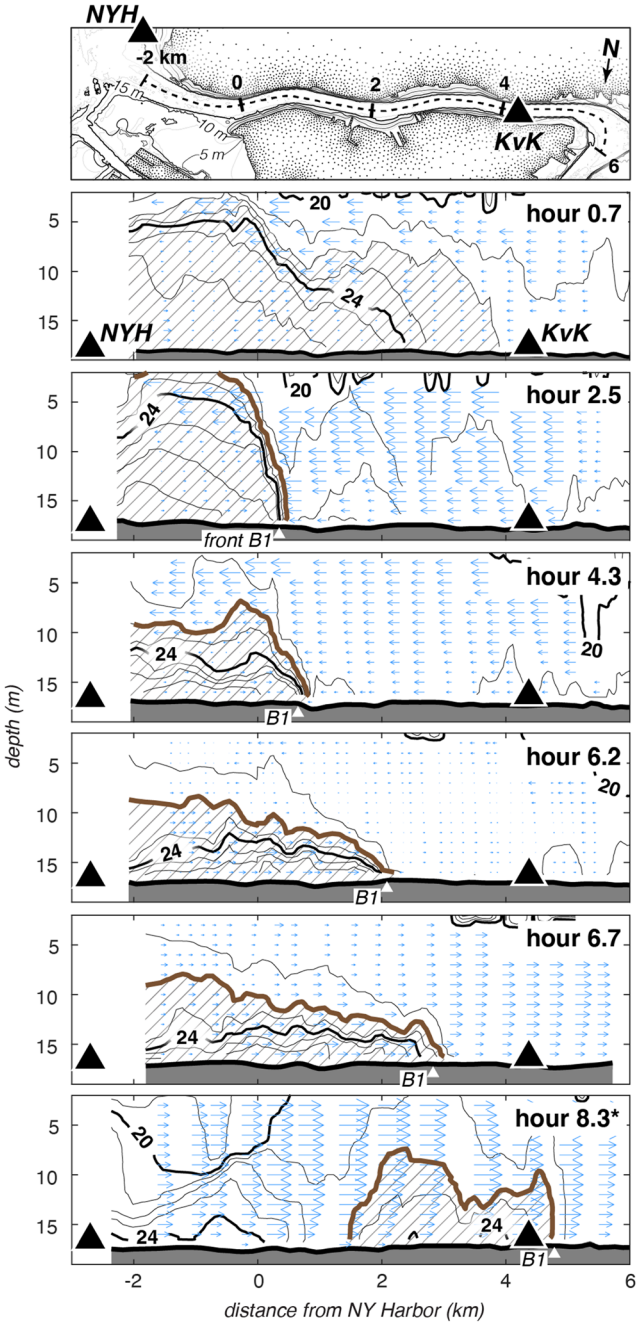

Fig. 5 Repeated along-channel salinity sections in Kill van Kull from the start of ebb tide (hour 0.7) through maximum flood (hour 8.3). Along-channel velocities are shown with arrows, and shading indicates salinities greater than 22 psu. The asterisk indicates that conditions at maximum flood were observed at the end of the previous tidal cycle

By maximum ebb (hour 2.5), this landward flow increases the salinity in New York Harbor by roughly 1 psu. Rapid ebb flow within Kill van Kull converges with the landward flow near 0 km at the newly formed front B1. The salinity difference across the front increases from 4 to 6 psu by late ebb (hour 4.3), despite a substantial decrease in the volume of saline water on the seaward side of the front. As ebb tide progresses, the front begins propagating landward as a gravity current,

traveling 2 km by the start of flood tide (hour 6.2). The Harbor continues to ebb through hour 6.7, isolating the propagating gravity current from a seaward source of salinity. The propagating front continues toward Newark Bay through the remainder of flood tide, passing mooring *KvK* (hour 8.3), and exiting the survey region.

The mechanism of formation of front B1 is shown in Fig. 6 through the components of the along-channel convergence term in the frontogenesis equation (term 3; Eq. 1). The front is initially observed as an along-channel salinity gradient maximum prior to maximum ebb tide (hour 2.5; Fig. 6). This salinity gradient maximum is concentrated by an along-channel velocity convergence at the mouth of the sub-estuary. Near-bed velocities reverse from − 0.5 m/s on the landward side of the front to + 0.1 m/s on the seaward side. This velocity convergence is generated by the response of stratified ebb flow to the seaward channel expansion at 0 km. The hydraulic state of flow within Kill van Kull is supercritical during ebb tide, and the lift-off of the isohaline associated with front B1 at the estuary—sub-estuary junction is consistent with the response of supercritical stratified flow to a channel expansion (MacDonald and Geyer 2005; Armi and Farmer 1986). This suggests that front B1 is generated by the hydraulic response of ebb flow to the junction. The front begins propagating landward by late ebb (hour 4.3), in response to weakening ebb velocities in Kill van Kull.

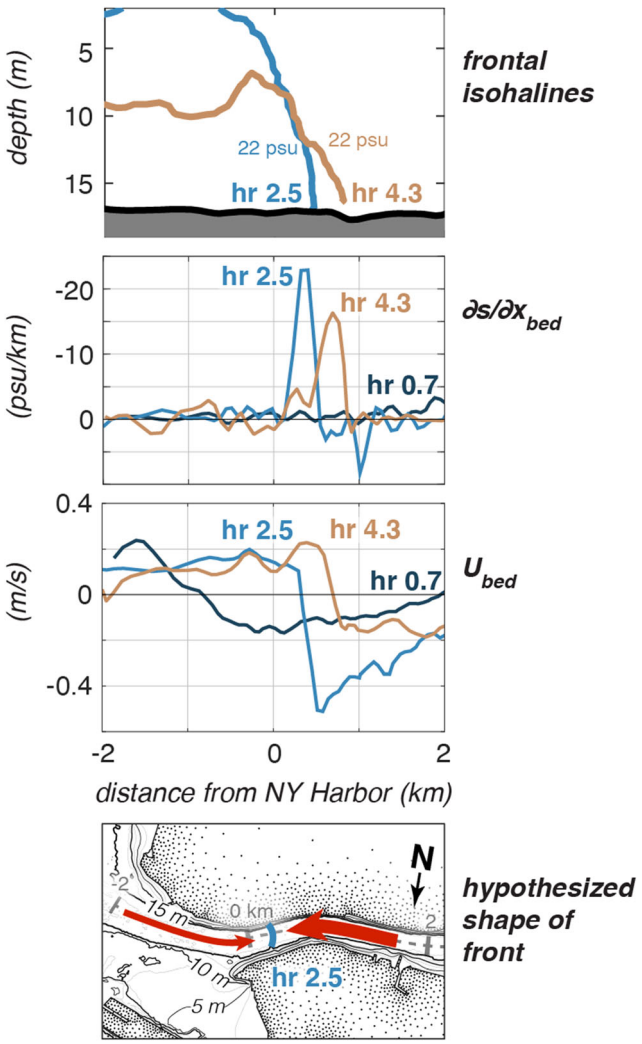

Fig. 6 Generation of bottom front B1 during ebb tide. The seaward channel expansion at the mouth of Kill van Kull is located at 0 km. Lines are labeled by tidal hour. Positive along-channel salinity gradients and velocities are directed landward. Arrows in the bottom panel indicate the directions of near-bed velocities during frontogenesis

Both the formation and propagation of front B1 are substantially influenced by the tidal velocity phase-shift between New York Harbor and the sub-estuary. During early ebb tide (hour 2.5; Fig. 5), the phase-shift juxtaposes saline, flood tide conditions in the Harbor with fresher, ebb tide conditions in the sub-estuary. This enhances the along-channel salinity and velocity gradients at the mouth of Kill van Kull, both of which enhance the along-channel salinity convergence. Because of the enhanced convergence, the front forms during early ebb; most lift-off fronts instead form during late ebb (Geyer and Ralston 2015). During early flood tide (hour 6.2), the phase-shift juxtaposes fresher, ebb tide conditions in the Harbor with saline, flood tide conditions in the sub-estuary. This reverses the near-bed salinity gradient at the mouth of Kill van Kull and detaches the propagating gravity current from New York Harbor (hour 8.3). The resulting isolated gravity current makes front B1 visibly different from the lift-off fronts observed at the mouths of salt wedge estuaries (Geyer and Farmer 1989; Ralston et al. 2010), which tend to have along-channel salinity gradients that monotonically increase toward the sea.

Front B2

The second bottom front is observed in Newark Bay; the tidal evolution of this front (front B2) is shown in Fig. 7 in roughly 90-min intervals from early ebb tide through maximum flood. A region of enhanced horizontal salinity gradient is observed near the mouth of a side channel at 10.5 km in early ebb tide (hour 1.5; Fig. 7); along-channel velocities in this region are weakly divergent. By maximum ebb (hour 3.0), the region is advected seaward, and a weak bottom front forms at this location (front B2). Near-bed velocities at front B2 are convergent; along-channel ebbing velocities on the landward side of the front are stronger than those on the seaward side. The weak initial salinity difference across the front increases to 1 psu by late ebb (hour 4.3), following a reduction of the salinity on the landward side of the front. The salinity on the seaward side of the front remains nearly constant. The front begins propagating landward by the start of flood (hour 6.2), passing mooring *NB* and exiting the survey region by maximum flood (hour 9.0).

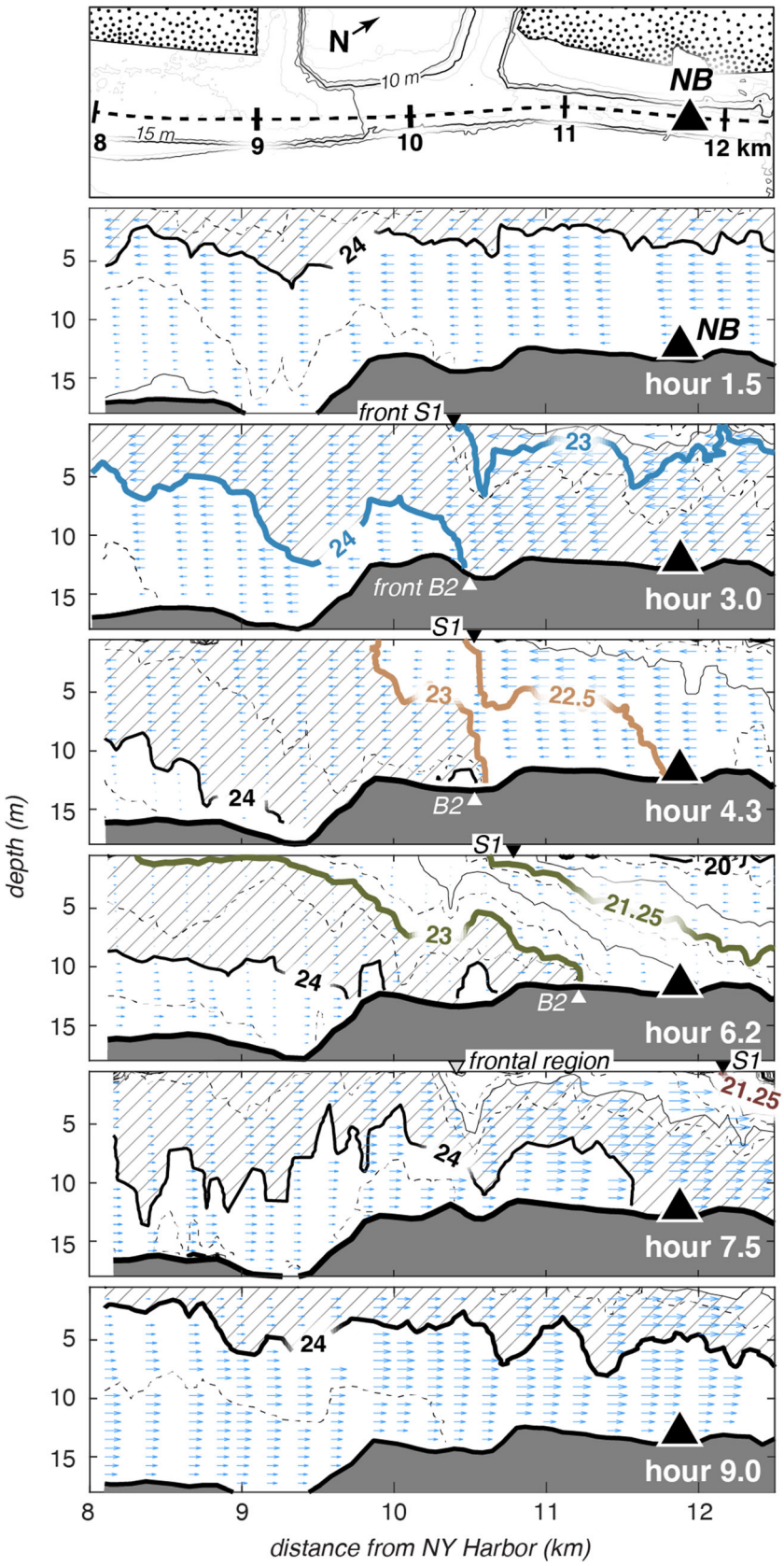

Fig. 7 Along-channel salinity sections in Newark Bay from early ebb tide (hour 1.5) through maximum flood (hour 9.0). Arrows indicate along-channel velocities, and shading corresponds to salinities between 23 and 24 psu. Isohalines associated with fronts B2 and S1 over time are highlighted with colors that correspond to the changes over time depicted in Figs. 8 and 10

The dynamics of front B2 appear to be related to two factors: the response of ebb flow to the seaward channel expansion at the mouth of the side channel at 10.5 km and the export of saline water from the same side channel. This is determined by analyses of along-channel variations of the horizontal salinity gradient, near-bed velocities, and repeated lateral hydrographic sections. Along-channel variations in the horizontal salinity gradient and near-bed velocities, the components of the along-channel convergence and cross-channel twisting terms in the frontogenesis equation (terms 3 and 4; Eq. 1) are shown during the formation of front B2 in Fig. 8. The front is first observed as a weak along-channel salinity gradient maximum at maximum ebb tide (hour 3.0; Fig. 8). The along-channel salinity gradient is drawn together by an along-channel velocity convergence at 10.5 km; ebbing near-bed velocities weaken by roughly 0.3 m/s over 500 m. We hypothesize that the velocity convergence is generated by the response of stratified ebb flow to the lateral channel expansion of the side channel junction, as ebb flow throughout the region is supercritical. The lack of a flow reversal across front B2 suggests that the front should be advected seaward. However, the front remains in nearly the same location through late ebb (hour 4.3).

Strong eastward lateral velocities on the seaward side of front B2 during late ebb tide suggest that the front is maintained and enhanced by the interaction of the main channel with the side channel (hour 4.3; Fig. 8). This is confirmed by repeated lateral hydrographic sections at the junction at a different time under similar environmental conditions (Fig. 9; note the lower salinity—the 20 psu isohaline roughly corresponds to the 24 psu isohaline in Fig. 7). The lateral sections are shown in roughly 90-min intervals from the end of flood tide through early flood tide. These sections reveal the presence of both baroclinic and barotropic tidal velocity phase-shifts between the main channel and side channel; flood tide persists in the side channel roughly 90 min after the start of ebb tide in the main channel. From the end of flood through early ebb tide (hours 11.8–1.3; Fig. 9), the near-bed salinity of the main channel is greater than the side channel. The combination of this baroclinic pressure gradient with a lateral barotropic pressure gradient generates a lateral circulation in which salt water is advected into the side channel from the main channel. The near-bed salinity in the main channel decreases as ebb tide progresses (hours 2.7–4.2), due to the seaward advection of fresh water from the Passaic and Hackensack rivers. By late ebb (hour 4.2), the low salinity of the main channel reverses the lateral near-bed baroclinic pressure gradient, which in turn reverses the circulation of the side channel. Consequently, salt water that was trapped in the side channel from the previous

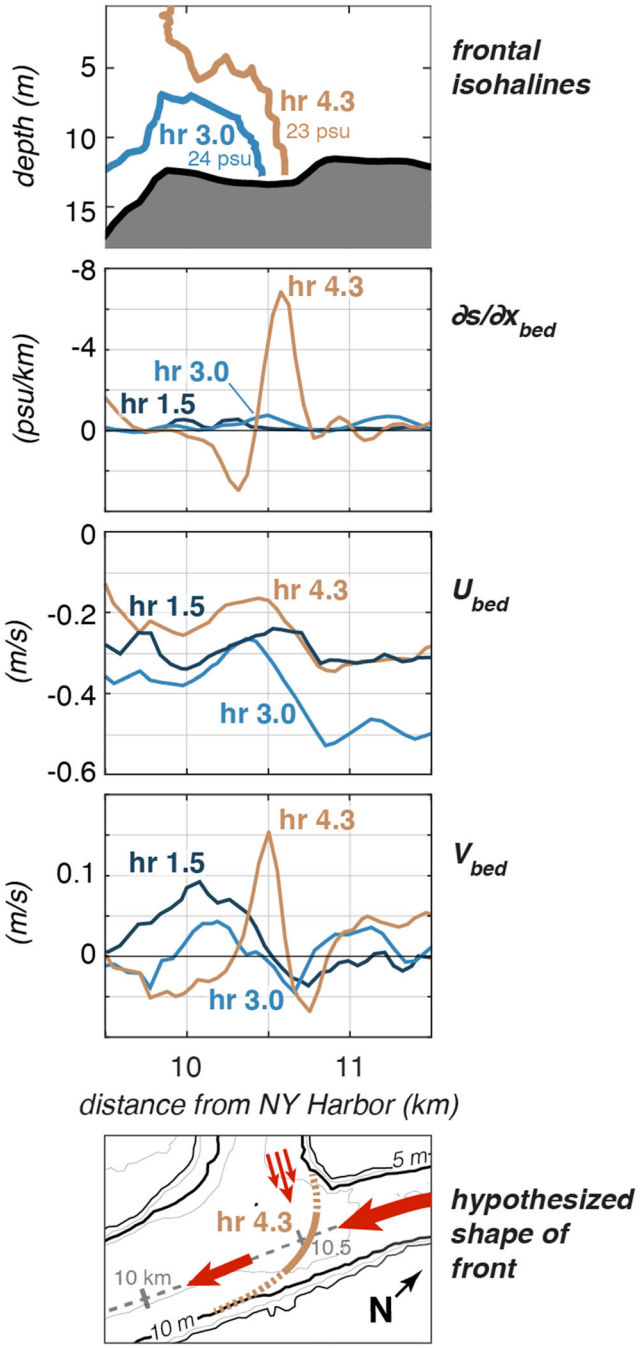

Fig. 8 Generation of front B2 during ebb tide. The mouth of the side channel is located at 10.5 km. Lines are labeled by tidal hour. Positive cross-channel salinity gradients and velocities are directed eastward (out of the page). Arrows in the bottom panel indicate the directions of near-bed velocities during frontogenesis

flood tide is expelled into the main channel. In Fig. 7, this is the bolus of 24 psu water on the seaward side of the front in late ebb (hours 4.3 and 6.2). The expulsion of salt water from the side channel continues through the end of ebb tide (hour 6.7; Fig. 9), maintaining the front as an oblique boundary between fresh water from upstream and salt water from the side channel.

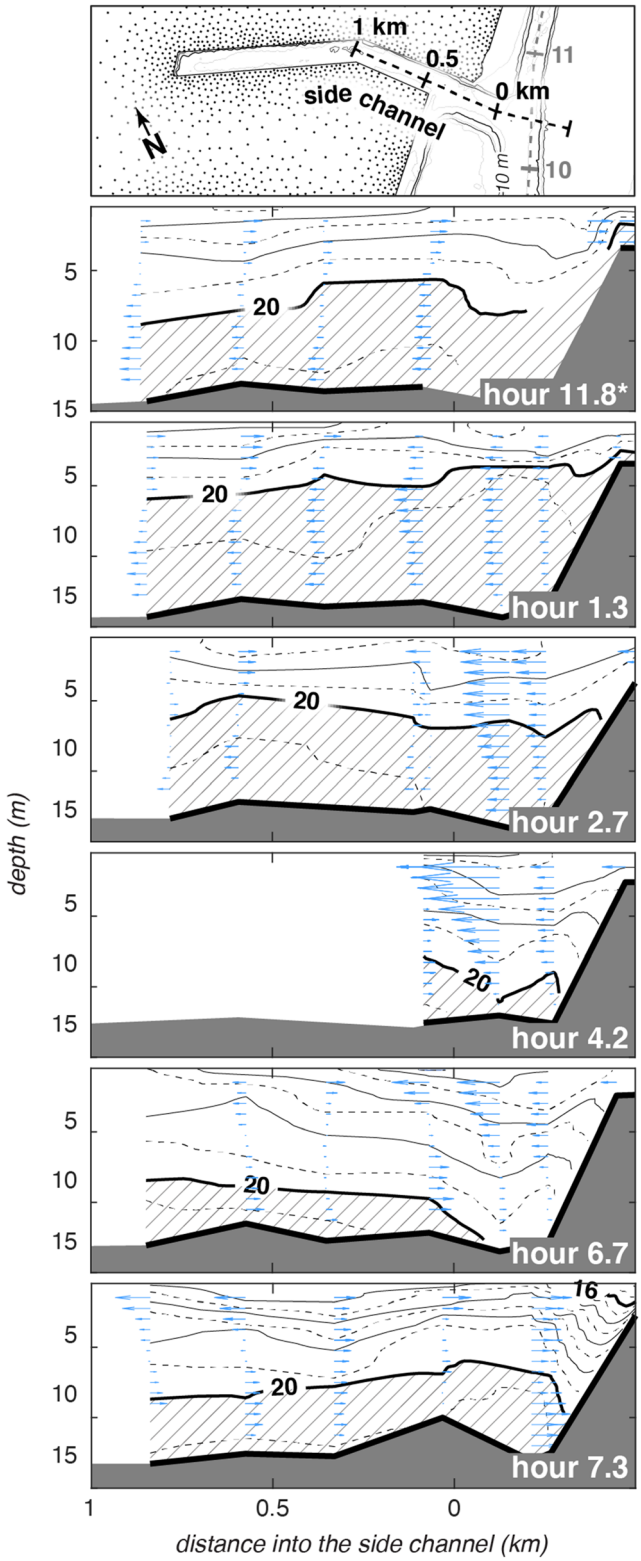

Fig. 9 Across-channel salinity sections in Newark Bay from the end of flood tide (hour 11.8) through early flood (hour 7.3). Arrows indicate across-channel velocities, and shading corresponds to salinities greater than 20 psu. The asterisk indicates that conditions at the end of flood tide were observed at the end of the depicted tidal cycle

Front S1

A surface front also forms during ebb tide at the seaward channel expansion at the mouth of the side channel (Fig. 7). In early ebb (hour 1.5), the surface velocities and salinity gradient throughout Newark Bay are nearly uniform. By maximum ebb (hour 3.0; Fig. 7), surface velocities roughly double on the landward side of the side channel at 10.5 km, whereas those on the seaward side remain nearly constant. This convergence is associated with the surface front (front S1). As ebb tide progresses (hour 4.3), the gradient zone remains in nearly the same location and retains a constant cross-front salinity difference, while the isohalines themselves are advected seaward. From maximum ebb to the end of ebb (hour 6.2), the isohaline associated with the front decreases from 23 to 21.25 psu. At the change of the tide, the front propagates landward, retaining the salinity, it was associated with at the end of ebb tide. By hour 7.5, the front passes mooring *NB*, as shown in Fig. 3. It continues landward and exits the survey region as flood tide progresses. After front S1 propagates landward, another surface front forms at the mouth of the side channel (hour 7.5). Although this front also propagates landward, it is stretched and weakened by the divergent surface velocity field at 11 km. Consequently, this second surface front in Newark Bay is dissipated by the time it passes mooring *NB* (hour 9.0).

We hypothesize that front S1 is generated by the response of along-channel flow to the lateral circulation of the side channel. This is suggested by analyses of along-channel variations of the horizontal salinity gradient and near-surface velocities—components of the along-channel convergence term in the frontogenesis equation (term 3; Eq. 1). The isohalines associated with front S1 during frontogenesis, as well as along-channel variations in the horizontal salinity gradient and near-surface velocities, are shown in Fig. 10. The front is first observed at maximum ebb tide as a weak maximum of the along-channel salinity gradient located above bottom front B2 at 10.5 km (hour 3.0; Fig. 10). The salinity gradient maximum is generated by an along-channel velocity convergence, in which surface velocities decrease by roughly 0.5 m/s over a distance of 500 m. The peak westward lateral velocities located at the along-channel convergence suggests that the surface convergence is generated by the interaction of the main channel with the side channel. This is confirmed by repeated hydrographic sections within the side channel during similar environmental conditions, shown in Fig. 9 from the end of flood tide through early flood tide.

At the end of flood tide (hour 11.8; Fig. 9), the surface salinity within the side channel is less than the salinity in the main channel. The resulting baroclinic pressure gradient generates a lateral circulation that exports fresh water from the side channel at the surface. However, this pressure gradient reverses as fresh water is advected seaward in the main

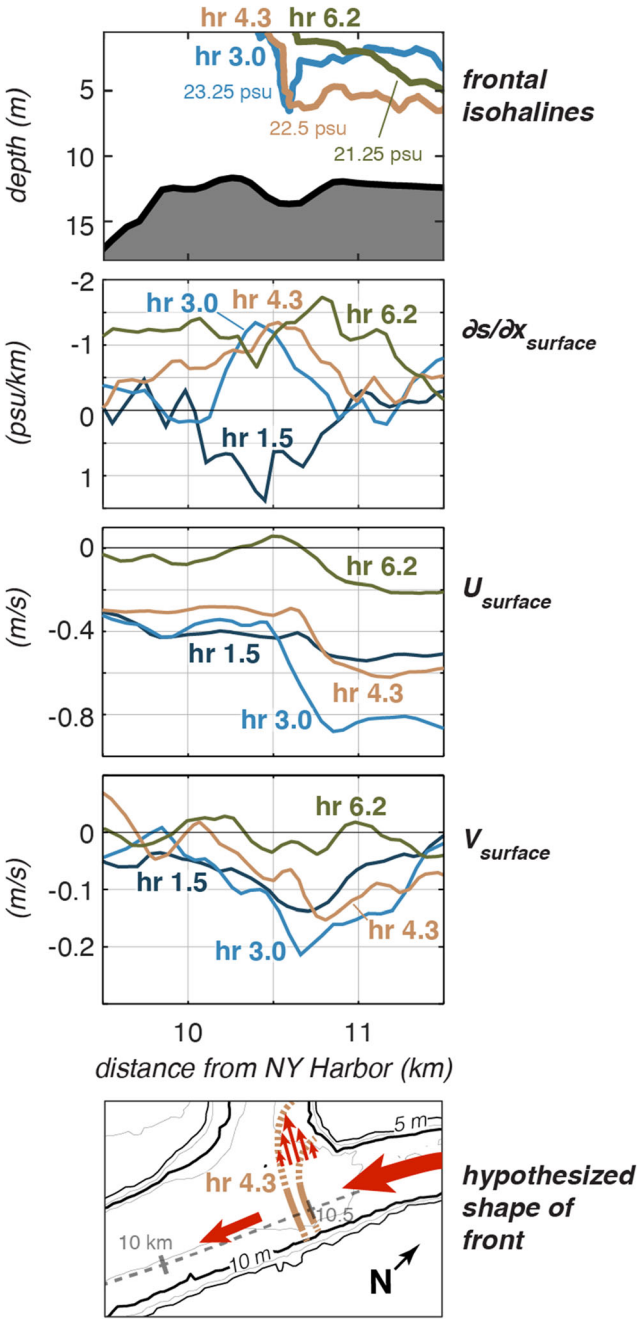

Fig. 10 Generation of front S1 during ebb tide. The mouth of the side channel is located at 10.5 km. Lines are labeled by tidal hour. Arrows in the bottom panel indicate the directions of near-surface velocities during frontogenesis

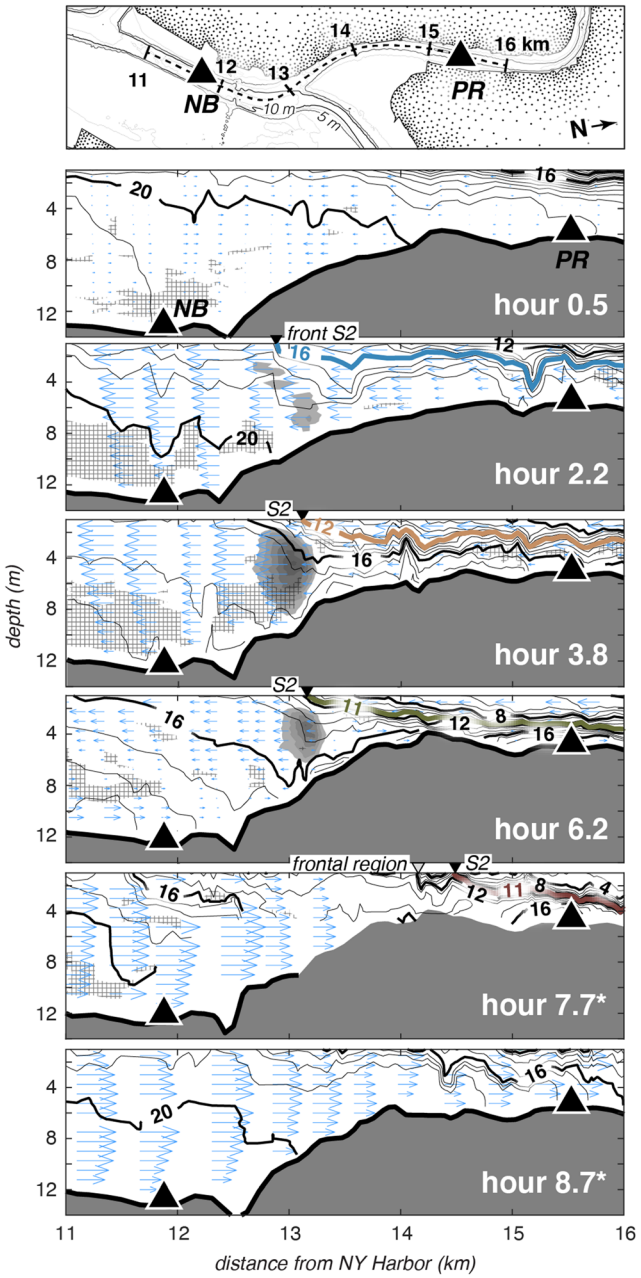

Fig. 11 Along-channel salinity sections at the mouth of the Passaic River from the start of ebb tide (hour 0.5) through maximum flood (hour 8.7). Arrows indicate along-channel velocities, and cross-hatching indicates regions in which the Richardson number is less than 0.5. Contours of westward cross-channel velocities, which emanate from the Hackensack River, are shown in 10 cm/s increments in gray; velocity contours start at 10 cm/s. Salinity isohalines associated with front S2 over time are shown with colors that correspond to the changes over time shown in Fig. 12

channel (hours 1.3–2.7). By maximum ebb tide (hour 2.7), the reversed baroclinic pressure gradient draws ebbing fresh water into the side channel, generating a weak lateral divergence in the main channel. The along-channel response to this lateral divergence is the weak surface velocity convergence that forms front S1 (hour 3.0; Fig. 10). Similar circulation patterns have been described before at the mouths of estuarine harbors (Langendoen and Karelse 1990), but the resulting along-channel surface front has not been reported. This circulation persists through the end of ebb tide (hours 4.2–6.7; Fig. 9), continuously concentrating the along-channel salinity gradient into a surface front at the mouth of side channel. With the change of tide (hour 6.2; Fig. 10), along-channel surface velocities on the seaward side of the front reverse direction, halting the seaward advection of fresh water. This couples the front to its end-of-ebb salinity and further draws surface

isohalines together, enhancing the front before it is advected landward.

Front S2

The strongest surface front observed in the Newark Bay system occurs at the mouth of the Passaic River; the formation and tidal evolution of this front (front S2) is shown in Fig. 11. At the start of ebb tide (hour 0.5), the surface salinity gradient increases from Newark Bay toward the Passaic. Weak surface velocities within Newark Bay are directed landward, and surface velocities within the Passaic are directed seaward. The resulting surface convergence forms a frontal region at 13 km. By maximum ebb (hour 2.2), this frontal region is advected seaward, and is replaced by surface front S2. This front is located above Hackensack River outflow, which is shown in Fig. 11 as a mid-depth cross-channel velocity maximum. As ebb tide progresses (hours 3.8–6.2), the front remains nearly stationary despite the seaward advection of surface isohalines; the salinity associated with the front decreases from 16 psu at maximum ebb to 11 psu at the end of ebb tide. With the change of tide, the front is advected landward and passes mooring *PR* by maximum flood (hour 8.7).

The dynamics of front S2 are associated with the merging of the Passaic and Hackensack rivers during ebb tide (Fig. 11). Because of the geometry of the confluence, Hackensack outflow impinges on outflow from the Passaic. The interaction between the two laterally convergent ebb flows was determined through analyses of the along-channel variations of the horizontal salinity gradient and near-surface velocities—components of the along-channel convergence and cross-channel gradient twisting terms in the frontogenesis equation (terms 3 and 4; Eq. 1). These components, as well as the front-associated isohalines, are shown in Fig. 12. The front is first observed in early ebb tide (hour 2.2; Fig. 12). Unlike the fronts described above, the along-channel velocity field at the location of front S2 is weakly divergent. Instead, the front is located in a region of cross-channel shear; westward lateral velocities peak immediately downstream of the front throughout ebb tide (hours 2.2–6.2). We hypothesize that this shear twists the boundary between the Passaic and Hackensack outflows into the along-channel direction. Throughout ebb tide, the magnitude of the along-channel salinity gradient at the front remains nearly constant. This is despite the tripling of cross-front shear from early ebb (hour 2.2) to the end of ebb tide (hour 6.2), which suggests that the strength of the front is not set by shear, but is instead set by the salinity gradient between the Passaic and Hackensack rivers. Consequently, the front is likely generated as a channel-parallel boundary between the two ebbing outflows and is rotated by the cross-channel shear to be oriented obliquely to the channel. This process is consistent with the formation of confluence fronts, which are generated by the along-channel straining of the interface between

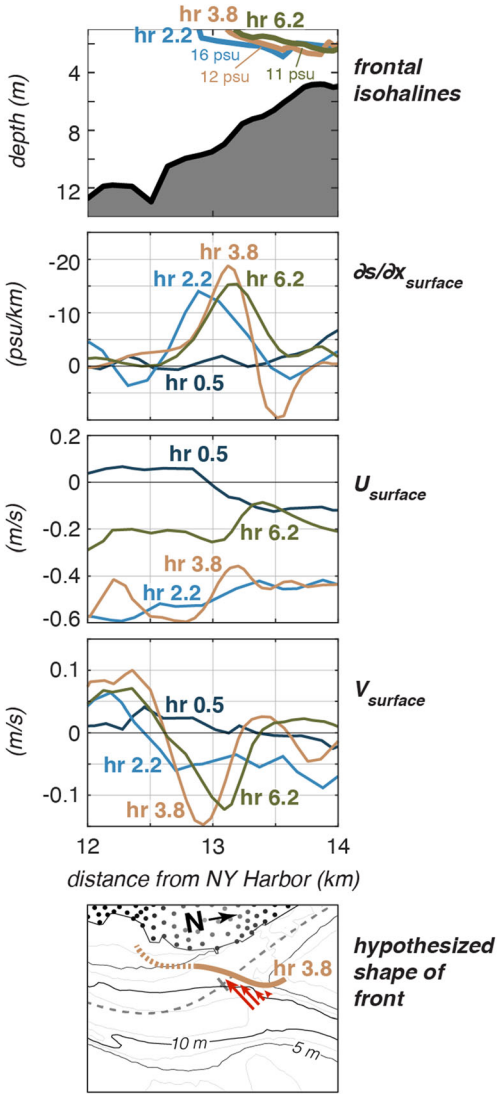

Fig. 12 Generation of front S2 during ebb tide. The mouth of the Passaic River is located at 13 km. Lines are labeled by tidal hour. Negative cross-channel velocities are directed westward (into the page). Arrows in the bottom panel indicate the directions of near-surface velocities during frontogenesis

convergent flows, and may be rotated into the along-channel direction by geometry-induced flow asymmetries (De Serres et al. 1999; Riley et al. 2014).

Front S2 is maintained by the confluence through the end of ebb, and like front S1, the salinity of the front steadily decreases throughout ebb tide. Although the lateral structure of the front was not resolved, the presence of the front within the along-channel sections in Fig. 11 demonstrates that the front extends over most of the mouth of the Passaic. This, combined with an absence of observations of unmixed fresh water further downstream, suggests that most ebbing fresh water from the Passaic passes through the front before being entrained into the saline and well-mixed Hackensack at the confluence. During late ebb (hour 3.8; Fig. 11), ebbing freshwater from the Passaic is entrained into the Hackensack near

the bed through a turbulent bottom boundary layer, which is shown by the region of low gradient Richardson number (Ri < 0.5) beneath the core of cross-channel velocities associated with the impinging Hackensack. Ebb flow from the Passaic is also entrained into the Hackensack at the surface; the lack of low gradient Richardson numbers near the surface suggests that Passaic fresh water is entrained into the Hackensack at the surface by horizontal mixing, such as through lateral shear instabilities along the front. When the tide turns to flood, the front is advected landward up the Passaic River, preserving the cross-front salinity difference between Passaic and Hackensack water.

Estuarine Heterogeneity Caused by Fronts

Over the course of the observation record, the fronts within the Newark Bay sub-estuary generate a heterogeneous along-channel salinity structure. Each front separates significantly different salinities during flood tide, as shown by histograms of the salinity distributions at each mooring location (Fig. 13). In addition, the mean flood tide salinity measured before front B1 is similar to the mean flood tide salinity observed after the passage of front B2 at mooring *NB*. The difference between the two means is less than one standard deviation, which indicates that the region between the two fronts is nearly homogeneous. This is also true for near-bed salinities observed before front B2 and near-surface salinities observed after front S1, as well as near-surface salinities observed before front S1 and after front S2. This shows that, on average, fronts divide the sub-estuary into three nearly homogeneous segments between New York Harbor and the Passaic River. These water masses can be thought of as Kill van Kull water (colored orange in Fig. 13), Newark Bay water (yellow in Fig. 13), and Hackensack confluence water (light teal in Fig. 13). The characterization of the sub-estuary as a segmented system is further supported by the heterogeneous along-channel structure of the sub-estuary observed at the end of ebb in Fig. 3. The horizontal density gradient is not continuously distributed along the sub-estuary during either flood or ebb phases of the tidal cycle. This indicates that Newark Bay has a tidally averaged structure that is more akin to a segmented fjord (e.g., Puget Sound; Ebbesmeyer and Barnes 1980) than to more uniform gradient estuaries, such as the main stem of the Hudson or James rivers (Haas 1977; Geyer et al. 2000). Because Newark Bay is segmented by fronts, this characterization may also be true for other frontal estuaries and may even be true at small horizontal scales for the more uniform gradient estuaries as well.

Discussion

This observational study demonstrates that along-channel salinity fronts are generated by tidal flow through geometric transitions and that these fronts contribute to along-channel estuarine heterogeneity. The relevant frontogenesis mechanisms have in many cases been described by previous studies (Best 1987; van Maren et al. 2009; Geyer and Ralston 2015); however, the dynamics at junctions within Newark Bay substantially modify fronts such that this study reveals important variations on classical ideas of frontogenesis.

Several types of fronts are described within the Newark Bay sub-estuary (Fig. 14). During ebb tide, a lift-off front (front B1) forms at the mouth of the sub-estuary from an along-channel convergence produced in response to the abrupt seaward channel expansion. A second lift-off front (front B2) similarly forms in response to an abrupt seaward expansion at the mouth of a side channel within the sub-

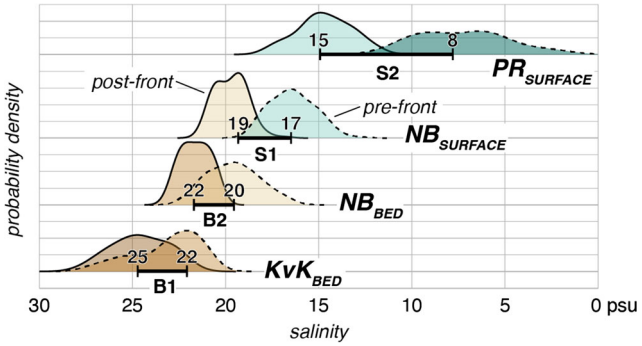

Fig. 13 Probability density functions of the average salinities measured before and after the passage of fronts during flood tides at moorings *KvK*, *NB*, and *PR*. In all cases, the average salinity measured during flood tide before the front (solid line density functions) is higher than the average salinity measured during flood tide after the front (dashed line density functions). Colors are used to emphasize observed water masses with similar mean values. Probability density is shown in increments of 0.1

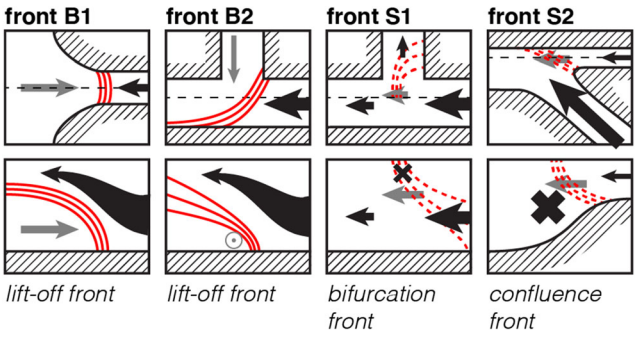

Fig. 14 Top- and side-view schematics of the formation of the observed fronts, showing velocities in black and isohalines in red. Dashed red lines indicate that the salinity associated with the front changes during ebb tide, whereas the isohalines depicted with solid lines remain nearly stationary. Gray arrows emphasize the unique aspects of each front. For fronts B1 and B2, these are the velocities produced by tidal velocity phase-shifts. For fronts S1 and S2, these represent the advected salinity field, which is decoupled from the location of the front

estuary. This front is maintained during late ebb by the export of high salinity water from the side channel. At the surface, ebbing fresh water is drawn into the side channel. This bifurcation of surface ebb flow generates an along-channel convergence, which in turn produces a surface front (front S1) above the lift-off front. We label this a bifurcation front; similar density-driven circulation patterns have been described at the mouths of harbors (e.g., Roelfzema and van Os 1978; Langendoen and Karelse 1990), but we are unaware of any descriptions of similar along-channel surface fronts. The strongest surface front—a confluence front (front S2)—is formed at the head of the sub-estuary by the merging of ebb flows at a channel confluence and is rotated across the mouth of the primary fresh water source by high velocities from the adjoining tributary estuary. Each of these four fronts is generated at a channel junction, and each front is also modified by either a tidal phase-shift or by the geometry of the junction.

An along-channel phase-shift at the mouth of the sub-estuary, for example, enhances the formation of lift-off front B1 (Fig. 14). These phase-shifts often occur due to transitions in channel geometry (Speer and Aubrey 1985; Friedrichs and Aubrey 1994). Both geometric transitions and along-channel phase-shifts are typically abrupt at junctions between short estuaries and the adjacent sea (Aubrey and Speer 1985), or sub-estuaries and the main estuary (Hayward et al. 1982; Roos and Schuttelaars 2015). In this study, the tidal phase of the sub-estuary leads the main estuary by 45°. Because the start of ebb tide in the sub-estuary occurs while the main estuary is at the end of flood tide, the phase-shift enhances the convergence of the along-channel salinity gradient at the mouth of the sub-estuary. This enhanced along-channel convergence initiates the early formation of lift-off front B1. As the front propagates landward during early flood tide, the phase-shift also detaches the gravity current behind front B1 from the main estuary. This occurs because the start of flood tide in the sub-estuary happens while the main estuary is at the end of ebb tide; the ebbing main estuary advects fresh water from a second source toward the mouth of the sub-estuary, which reverses the along-channel salinity gradient at the junction. The effects of the phase-shift on both frontogenesis and frontal evolution make this lift-off front different from others described at the mouths of estuaries, such as the fronts described by Geyer and Farmer (1989) and Ralston et al. (2010). Because tidal phase-shifts are common at junctions which are also conducive to frontogenesis, we suspect that many lift-off fronts are modified in a manner similar to the front described in this study.

Within the sub-estuary, along-channel fronts are modified by lateral barotropic and baroclinic tidal velocity phase-shifts at a channel—side channel junction. Lateral phase-shifts often occur between channels of different geometries (Warner et al. 2002), or of different lengths (van Maren et al. 2009). de Nijs et al. (2009) described how these phase-shifts set up fronts that propagate into side channels; this study finds that lateral phase-shifts also generate fronts within the main channel. During ebb tide, the salinity gradient between fresh water in the main channel and salt water in the side channel induces a lateral circulation that expels salt water into the main channel at the bed, similar to a lock exchange. The expelled salt water maintains bottom front B2, which forms at the seaward expansion of the side channel (Fig. 14). At the same time, the lateral circulation draws fresh water into the side channel, producing a lateral flow divergence at the surface. This induces an along-channel convergence, which forms surface front S1 above bottom front B2 (Fig. 14). This scenario appears to be unique to channel—side channel junctions, as most seaward channel expansions exhibit divergent along-channel surface velocities during ebb tide (e.g., Luketina and Imberger 1987). The process may also require a minimum along-channel salinity gradient at the junction. The southern side channel in Newark Bay, for example, is of similar dimensions to the northern side channel but does not generate a lateral lock exchange, likely due to the smaller tidal salinity range in the deeper, southern half of the sub-estuary. In any case, the fronts resulting from the exchange with the side embayment contribute to the along-channel heterogeneity of the sub-estuary, consistent with their contribution to along-channel dispersion due to tidal trapping, as discussed by Okubo (1973) and MacVean and Stacey (2010).

This study also identified fronts that are generated by the geometry of confluence junctions. While they have been previously associated with river confluences (Best 1987; Rhoads and Kenworthy 1995), such fronts may be quite common in estuaries. The front described by this study (front S2; Fig. 14), as well as similar fronts described by Redbourn (1996) and Giddings et al. (2012), demonstrates that such fronts form in estuaries at junctions between channels as well as between a channel and side embayment. The buoyancy gradients across these fronts are induced by different sources of salinity, or by a tidal velocity phase-shift. Farmer et al. (1995) describe a similar front at a barotropic confluence of tidal flows in the Strait of Georgia—Juan de Fuca Strait system. This front is characterized by a frontal interface that is strained by the local velocity field, and numerical model results indicate that the convergence originates at the coast of Stuart Island. This suggests that the front is generated by the confluence of flows around the island rather than by local shear. The plume front described at the mouth at the Connecticut River by O'Donnell (1990) and Garvine (1977) also shares similar characteristics with a confluence front, in that it is generated at a boundary between

laterally convergent flows with different salinity sources. Although these examples suggest that confluence fronts may be widespread in estuaries, further studies are needed to clarify the prevalence of fronts formed by lateral convergences and interfacial strain at confluences.

By forming and modifying fronts, the geometric transitions at junctions divide the estuary into a series of distinct, nearly homogeneous segments on tidal timescales. The segmented structure of the sub-estuary is suggested by the overall hydrographic section at the end of ebb tide and confirmed by measurements of similar salinities between fronts during flood tide. The presence of along-channel heterogeneity during both flood and ebb phases of the tidal cycle indicate that the sub-estuary is continually divided into distinct segments between sites of abrupt geometric transition. The analyses of shipboard hydrography revealed that these sites within the Newark Bay sub-estuary form fronts.

The division of an estuary by fronts may be a common feature of partially mixed and well-mixed estuaries. Geyer and Ralston's (2015) study of fronts in the Hudson estuary found that fronts can be generated by relatively small changes in geometry, and this study finds that even small differences in salinity across fronts may represent the major part of the along-estuary salinity variation. This suggests that the tidally averaged along-channel gradients, and perhaps even the mean circulation, of frontal estuaries are more similar to geometrically segmented fjords (e.g., Puget Sound; Cokelet and Stewart 1985) than to the idealized partially mixed estuaries often described in the literature (Hansen and Rattray Jr. 1965; MacCready and Geyer 2010).

Acknowledgments We thank David Ralston for helpful discussions and comments on this manuscript. The observations and much of the analysis were supported by National Science Foundation grant OCE-1325136. Additional support for the analysis and the preparation of the manuscript was provided by Hudson River Foundation Graduate Fellowship GF/01/17 and the J. Seward Johnson Fund at Woods Hole Oceanographic Institution.

References

Alebregtse, N.C., H.E. de Swart, and H.M. Schuttelaars. 2013. Resonance characteristics of tides in branching channels. *Journal of Fluid Mechanics* 728: R3. https://doi.org/10.1017/jfm.2013.319.

Allen, F.H., and W.A. Price. 1959. Density currents and siltation in docks and tidal basins. *The Dock and Harbour Authority* 40 (465): 72–76.

Armi, L., and D.M. Farmer. 1986. Maximal two-layer exchange through a contraction with barotropic net flow. *Journal of Fluid Mechanics* 164: 27–51. https://doi.org/10.1017/s0022112086002458.

Aubrey, D.G., and P.E. Speer. 1985. A study of non-linear tidal propagation in shallow inlet/estuarine systems part I: observations. *Estuarine, Coastal and Shelf Science* 21 (2): 185–205. https://doi.org/10.1016/0272-7714(85)90096-4.

Benjamin, T.B. 1968. Gravity currents and related phenomena. *Journal of Fluid Mechanics* 31 (02): 209–248. https://doi.org/10.1017/s0022112068000133.

Best, J.L. 1987. Flow dynamics at river channel confluences: implications for sediment transport and bed morphology. *Recent Developments in Fluvial Sedimentology* SP39: 27–35. https://doi.org/10.2110/pec.87.39.0027.

Blumberg, A.F., L.A. Khan, and J.P. St John. 1999. Three-dimensional hydrodynamic model of New York Harbor region. *Journal of Hydraulic Engineering* 125 (8): 799–816. https://doi.org/10.1061/jhend8.1999.125.issue-8;page:string:Article/Chapter.

Brubaker, J.M., and J.H. Simpson. 1999. Flow convergence and stability at a tidal estuarine front: acoustic Doppler current observations. *Journal of Geophysical Research: Oceans* 104 (C8): 18257–18268. https://doi.org/10.1029/1999JC900117.

Chant, R.J., D.C. Fugate, and E. Garvey. 2011. The shaping of an estuarine superfund site: roles of evolving dynamics and geomorphology. *Estuaries and Coasts* 34 (1): 90–105. https://doi.org/10.1007/s12237-010-9324-z.

Chant, R.J., C.K. Sommerfield, and S.A. Talke. 2018. Impact of channel deepening on tidal and gravitational circulation in a highly engineered estuarine basin. *Estuaries and Coasts* 73 (3): 587–1600. https://doi.org/10.1007/s12237-018-0379-6.

Cokelet, E.D., and R.J. Stewart. 1985. The exchange of water in fjords: the efflux/reflux theory of advective reaches separated by mixing zones. *Journal of Geophysical Research: Oceans* 90 (C4): 7287–7306. https://doi.org/10.1029/JC090iC04p07287.

De Serres, B., A.G. Roy, P.M. Biron, and J.L. Best. 1999. Three-dimensional structure of flow at a confluence of river channels with discordant beds. *Geomorphology* 26 (4): 313–335. https://doi.org/10.1016/s0169-555x(98)00064-6.

Ebbesmeyer, C.C., and C.A. Barnes. 1980. Control of a fjord basin's dynamics by tidal mixing in embracing sill zones. *Estuarine and Coastal Marine Science* 11 (3): 311–330. https://doi.org/10.1016/s0302-3524(80)80086-7.

Farmer, D.M., E.A. D'Asaro, M.V. Trevorrow, and G.T. Dairiki. 1995. Three-dimensional structure in a tidal convergence front. *Continental Shelf Research* 15 (13): 1649–1673. https://doi.org/10.1016/0278-4343(94)00084-Z.

Friedrichs, C.T., and D.G. Aubrey. 1994. Tidal propagation in strongly convergent channels. *Journal of Geophysical Research* 99 (C2): 3321. https://doi.org/10.1029/93jc03219.

Garvine, R.W. 1977. Observations of the motion field of the Connecticut River plume. *Journal of Geophysical Research: Oceans* 82 (3): 441–454. https://doi.org/10.1029/JC082i003p00441.

Geyer, W.R., and D.M. Farmer. 1989. Tide-induced variation of the dynamics of a salt wedge estuary. *Journal of Physical Oceanography* 19 (8): 1060–1072. https://doi.org/10.1175/1520-0485(1989)019<1060:TIVOTD>2.0.CO;2.

Geyer, W.R., and D.K. Ralston. 2015. Estuarine frontogenesis. *Journal of Physical Oceanography* 45 (2): 546–561. https://doi.org/10.1175/JPO-D-14-0082.1.

Geyer, W.R., J.H. Trowbridge, and M.M. Bowen. 2000. The dynamics of a partially mixed estuary. *Journal of Physical Oceanography* 30 (8): 2035–2048. https://doi.org/10.1175/1520-0485(2000)030<2035:tdoapm>2.0.co;2.

Giddings, S.N., D.A. Fong, S.G. Monismith, C.C. Chickadel, K.A. Edwards, W.J. Plant, B. Wang, O.B. Fringer, A.R. Horner-Devine, and A.T. Jessup. 2012. Frontogenesis and frontal progression of a trapping-generated estuarine convergence front and its influence on mixing and stratification. *Estuaries and Coasts* 35 (2): 665–681. https://doi.org/10.1007/s12237-011-9453-z.

Haas, L.W. 1977. The effect of the spring-neap tidal cycle on the vertical salinity structure of the James, York and Rappahannock rivers, Virginia, USA. *Estuarine and Coastal Marine Science* 5 (4): 485–496. https://doi.org/10.1016/0302-3524(77)90096-2.

Hansen, D.V., and M. Rattray Jr. 1965. Gravitational circulation in straits and estuaries. *Journal of Marine Research* 23 (2): 104–122.

Hayward, D., C.S. Welch, and L.W. Haas. 1982. York River destratification: an estuary-subestuary interaction. *Science* 216 (4553): 1413–1414. https://doi.org/10.1126/science.216.4553.1413.

Horner-Devine, A.R., R.D. Hetland, and D.G. MacDonald. 2015. Mixing and transport in coastal river plumes. *Annual Review of Fluid Mechanics* 47 (1): 569–594. https://doi.org/10.1146/annurev-fluid-010313-141408.

Huzzey, L.M. 1982. The dynamics of a bathymetrically arrested estuarine front. *Estuarine, Coastal and Shelf Science* 15 (5): 537–552. https://doi.org/10.1016/0272-7714(82)90005-1.

Kaluarachchi, I. D., M. S. Bruno, Q. Ahsan, A. F. Blumberg, and H. Li. 2003. Estimating the volume and salt fluxes through Arthur Kill and the Kill van Kull. In World Water Environmental Resources Congress 2003, 1–10. Philadelphia, PA: American Society of Civil Engineers. https://doi.org/10.1061/40685(2003)225.

Langendoen, E. J., and M. Karelse. 1990. Laboratory observations of velocity and density fields in the entrance of a harbor on a stratified tidal river. 1–90. Delft: TU Delft, Department of Hydraulic Engineering; TU Delft, Department of Hydraulic Engineering.

Largier, J.L. 1992. Tidal intrusion fronts. *Estuaries* 15 (1): 26–39. https://doi.org/10.2307/1352707.

Largier, J.L. 1993. Estuarine fronts: how important are they? *Estuaries* 16 (1): 1–11. https://doi.org/10.2307/1352760.

Lavelle, J.W., E.D. Cokelet, and G.A. Cannon. 1991. A model study of density intrusions into and circulation within a deep, silled estuary: Puget Sound. *Journal of Geophysical Research* 96 (C9): 16779. https://doi.org/10.1029/91jc01450.

Luketina, D.A., and J. Imberger. 1987. Characteristics of a surface buoyant jet. *Journal of Geophysical Research: Earth Surface* 92 (C5): 5435–5447. https://doi.org/10.1029/JC092iC05p05435.

MacCready, P., and W.R. Geyer. 2010. Advances in estuarine physics. *Annual Review of Marine Science* 2 (1): 35–58. https://doi.org/10.1146/annurev-marine-120308-081015.

MacDonald, D.G., and W.R. Geyer. 2005. Hydraulic control of a highly stratified estuarine front. *Journal of Physical Oceanography* 35 (3): 374–387. https://doi.org/10.1175/jpo-2692.1.

MacVean, L.J., and M.T. Stacey. 2010. Estuarine dispersion from tidal trapping: a new analytical framework. *Estuaries and Coasts* 34 (1): 45–59. https://doi.org/10.1007/s12237-010-9298-x.

van Maren, D.S., J.C. Winterwerp, and M. Sas. 2009. The effect of dock length on harbour siltation. *Continental Shelf Research* 29 (11–12): 1410–1425. https://doi.org/10.1016/j.csr.2009.03.003.

Marmorino, G.O., and C.L. Trump. 1996. High-resolution measurements made across a tidal intrusion front. *Journal of Geophysical Research: Oceans* 101 (C11): 25661–25674. https://doi.org/10.1029/96jc02384.

Mathew, R., and J.C. Winterwerp. 2017. Surficial sediment erodibility from time-series measurements of suspended sediment concentrations: development and validation. *Ocean Dynamics* 67 (6): 691–712. https://doi.org/10.1007/s10236-017-1055-2.

Nepf, H.M., and W.R. Geyer. 1996. Intratidal variations in stratification and mixing in the Hudson estuary. *Journal of Geophysical Research: Oceans* 101 (C5): 12079–12086. https://doi.org/10.1029/96JC00630.

de Nijs, M.A.J., J.C. Winterwerp, and J.D. Pietrzak. 2009. On harbour siltation in the fresh-salt water mixing region. *Continental Shelf Research* 29 (1): 175–193. https://doi.org/10.1016/j.csr.2008.01.019.

Nunes, R. A. 1982. The dynamics of small-scale fronts in estuaries. PhD thesis, Anglesey: University of Wales; University of Wales. http://ethos.bl.uk/OrderDetails.do?uin=uk.bl.ethos.324329.

O'Donnell, J. 1990. The formation and fate of a river plume: a numerical model. *Journal of Physical Oceanography* 20 (4): 551–569. https://doi.org/10.1175/1520-0485(1990)020<0551:tfafoa>2.0.co;2.

Okubo, A. 1973. Effect of shoreline irregularities on streamwise dispersion in estuaries and other embayments. *Netherlands Journal of Sea Research* 6 (1–2): 213–224. https://doi.org/10.1016/0077-7579(73)90014-8.

Pelegri, J.L. 1988. Tidal fronts in estuaries. *Estuarine, Coastal and Shelf Science* 27 (1): 45–60. https://doi.org/10.1016/0272-7714(88)90031-5.

Pritchard, D. W., and R. E. Bunce. 1959. Physical and chemical hydrography of the Magothy River. 17. Baltimore, MD: Johns Hopkins University; Chesapeake Bay Institute.

Ralston, D.K., W.R. Geyer, and J.A. Lerczak. 2010. Structure, variability, and salt flux in a strongly forced salt wedge estuary. *Journal of Geophysical Research: Oceans* 115 (C6): C06005–C06021. https://doi.org/10.1029/2009JC005806.

Redbourn, L. J. 1996. The structure and dynamics of a convergent estuarine front. PhD thesis, Plymouth, UK: University of Plymouth; University of Plymouth. http://hdl.handle.net/10026.1/1809.

Rhoads, B.L., and S.T. Kenworthy. 1995. Flow structure at an asymmetrical stream confluence. *Geomorphology* 11 (4): 273–293. https://doi.org/10.1016/0169-555x(94)00069-4.

Rhoads, B.L., and A.N. Sukhodolov. 2001. Field investigation of three-dimensional flow structure at stream confluences: 1. Thermal mixing and time-averaged velocities. *Water Resources Research* 37 (9): 2393–2410. https://doi.org/10.1029/2001wr000316.

Riley, J.D., B.L. Rhoads, D.R. Parsons, and K.K. Johnson. 2014. Influence of junction angle on three-dimensional flow structure and bed morphology at confluent meander bends during different hydrological conditions. *Earth Surface Processes and Landforms* 40 (2): 252–271. https://doi.org/10.1002/esp.3624.

Roelfzema, A., and A. G. van Os. 1978. Effect of harbours on salt intrusion in estuaries. In *International Conference on Coastal Engineering*, 2810–26. Hamburg: American Society of Civil Engineers; American Society of Civil Engineers. doi:https://doi.org/10.1061/9780872621909.174.

Roos, P.C., and H.M. Schuttelaars. 2015. Resonance properties of tidal channels with multiple retention basins: role of adjacent sea. *Ocean Dynamics* 65 (3): 311–324. https://doi.org/10.1007/s10236-015-0809-y.

Shrestha, P., S. Su, S. James, P. Shaller, M. Doroudian, C. Firstenberg, and C. Thompson. 2014. Conceptual site model for Newark Bay—hydrodynamics and sediment transport. *Journal of Marine Science and Engineering* 2 (1): 123–139. https://doi.org/10.3390/jmse2010123.

Simpson, J.E., and P.F. Linden. 1989. Frontogenesis in a fluid with horizontal density gradients. *Journal of Fluid Mechanics* 202: 1–16. https://doi.org/10.1017/s0022112089001072.

Simpson, J.H., and R.A. Nunes. 1981. The tidal intrusion front: an estuarine convergence zone. *Estuarine, Coastal and Shelf Science* 13 (3): 257–266. https://doi.org/10.1016/S0302-3524(81)80024-2.

Speer, P.E., and D.G. Aubrey. 1985. A study of non-linear tidal propagation in shallow inlet/estuarine systems. Part II: theory. *Estuarine, Coastal and Shelf Science* 21 (2): 207–224. https://doi.org/10.1016/0272-7714(85)90097-6.

Suszkowski, D. J. 1978. Sedimentology of Newark Bay, New Jersey. PhD thesis, Newark, DE: University of Delaware; University of Delaware.

Warner, J.C., D.H. Schoellhamer, J.R. Burau, and S.G. Schladow. 2002. Effects of tidal current phase at the junction of two straits. *Continental Shelf Research* 22 (11–13): 1629–1642. https://doi.org/10.1016/S0278-4343(02)00026-2.

Warner, J.C., D.H. Schoellhamer, and S.G. Schladow. 2003. Tidal truncation and barotropic convergence in a channel network tidally driven from opposing entrances. *Estuarine, Coastal and Shelf Science* 56 (3–4): 629–639. https://doi.org/10.1016/S0272-7714(02)00213-5.